Article

Tailoring an Effective Interface between Nanocellulose and the Epoxidized Linseed Oil Network through Functionalization

Mădălina I. Necolau, Brîndușa Bălănucă, Adriana N. Frone, and Celina M. Damian*

Read Online

ACCESS | Metrics & More | Article Recommendations

ABSTRACT: Sustainable nanocomposite materials based on different functionalized nanocellulose (NC) structures embedded in epoxidized linseed oil (ELO) were developed as foundation toward a greener approach for anticorrosive coating evolution. The work leans on functionalization with (3-aminopropyl) triethoxysilane (APTS), (3-glycidyloxypropyl)trimethoxysilane (GPTS), and vanillin (V) of NC structures isolated from plum seed shells, evaluated as potential reinforcing agents for the increase of thermomechanical properties and water resistance of epoxy nanocomposites from renewable resources. The successful surface modification was confirmed from the deconvolution of X-ray photoelectron spectra for C 1s and correlated with Fourier transform infrared (FTIR) data. The secondary peaks assigned to C−O−Si at 285.9 eV and C−N at 286 eV were observed with the decrease of the C/O atomic ratio. Compatibility and efficient interface formation between the functionalized NC and the biobased epoxy network from linseed oil were translated as decreased values for the surface energy of bio-nanocomposites and better dispersion imaged through scanning electron microscopy (SEM). Thus, the storage modulus of the ELO network reinforced with only 1% APTS-functionalized NC structures reached 5 GPa, an almost 20% increase compared with that of the neat matrix. Mechanical tests were applied to assess an increase of 116% in compressive strength for the addition of 5 wt % NCA to the bioepoxy matrix.
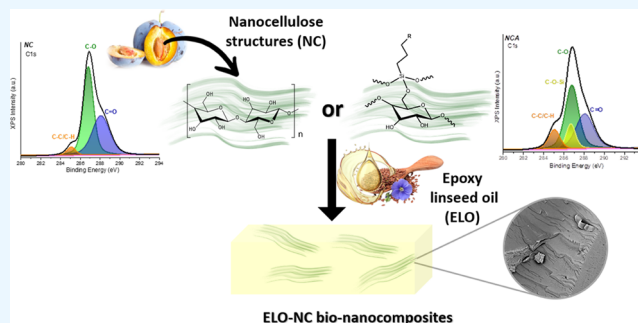
INTRODUCTION

The development of sustainable polymeric materials has become a subject of great interest considering the level of pollution worldwide, the depletion of fossil resources, and the huge potential offered by renewable resources, which can be considered for the fabrication of various products.

Vegetable oils (VO) such as epoxidized soybean oil (ESO),[1] epoxidized castor oil (ECO),[2] and epoxidized linseed oil (ELO)[3] have proved to be valuable compounds to design polymeric matrices that can be further involved to obtain multivalent composite or hybrid materials with a wide applicability in the industrial field.

Nanocellulose (NC) is a nanostructured compound[4,5] resulting from the cellulose reworking, with cellulose being one of the most abundant natural resources easy to isolate from wood, fibers, and various byproducts and waste from important industries[6] (e.g., food processing industry, agriculture,[7] and packaging). Due to its outstanding properties such as high specific surface area and superior mechanical properties,[8] NC was employed in many studies conducted toward the development of green or sustainable nanocomposite materials. Up to now, NC has been used in composite formulations based on different polymers including poly(vinyl alcohol) (PVA),[9] polyurethane,[10] epoxy resin,[11] poly(lactic acid),[12] polyethylene,[13] and polypropylene.[14]

Nevertheless, NC-based nanomaterials possess specific shortcomings; the main drawbacks come from the incompatibility of the hydrophilic filler with the hydrophobic polymers, which will consequently lead to difficulties in terms of dispersion[15,16]

A very important issue that needs to be considered when developing nanocomposites is the interfacial interaction of the continuous polymeric phase and the nanofiller and also the compatibility of the components.[17,18] To overcome the above-mentioned limitations, a suitable strategy would be the NC surface functionalization to reduce the hydrophilicity of the cellulose derivative and to achieve superior properties for the final materials.[19,20] The multiple OH functionalities from the NC surface represent valuable reactive sites for further
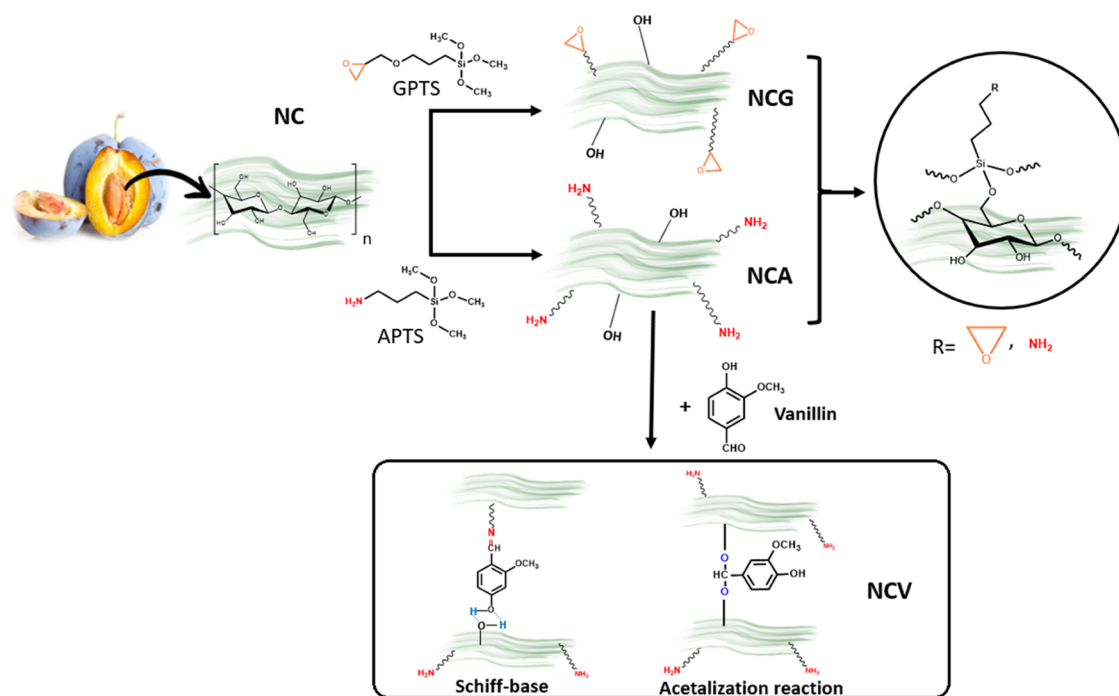
Figure 1. Schematic illustration of the chemical structure of functionalized NC.

chemical modification in order to attain an adequate interface with respect to the hydrophobic polymer matrix, so better properties can be achieved.[21] Among the reported surface modifications from the literature silane treatment,[22] oxidation[23] and esterification[24] proved to be valuable approaches to increase the compatibility of NC with the epoxy matrix.

Pacaphol and Aht-Ong[25] studied the influence of silane-modified NC for coating development, establishing that the amino-silane decoration of the cellulose derivative can enhance the adhesion on various substrates and the hardness and hydrophobic character. A study conducted by Roszowska-Jarosz[26] investigated the influence of the NC content in conventional epoxy nanocomposites from 0.5 to 1.5% (w/w). Superior mechanical properties were achieved in the case of 1% NC content, while the highest value of destruction energy was recorded for the nanocomposite containing 0.5% NC.

Kuo et al.[27] developed advanced bio-nanocomposites by reinforcing hybrid biobased epoxy and petroleum-based monomer systems with NC fibers. SEM analyses indicate a sequential interaction of the NC fibers with the polymeric matrix, which was further correlated with the superior mechanical properties (85 MPa for tensile strength and 4.6 GPa for tensile modulus).

Wang and co-workers[28] used ureido-pyrimidinone (UPy) to functionalize the nanocellulose (NC) surface to decrease self-aggregation and to improve the interfacial compatibility with the epoxy resin for the development of advanced nanocomposites. The morphological analysis revealed that the NC-UPy dispersed uniformly in the polymeric matrix, showing a good interfacial compatibility, leading to an 87% increase in the tensile strength of the formed nanocomposite membrane when the tensile strength of the composite material with 0.5 wt % NCC-UPy showed an 87% increase in comparison with the neat sample, thus demonstrating the outstanding reinforcing effect of the functionalized nanocellulose.

In terms of VO-based epoxy nanocomposite materials, there are few studies that deal with the incorporation of cellulose derivatives to generate biobased thermoset materials with great properties. Sunflower oil-derived epoxy polymers containing cellulose nanocrystals (CNCs) were recently studied.[29] Superior properties were achieved by creating an adequate interfacial hydrogen bonding, resulting in high compatibility between the polymeric matrix and filler.

Thus, the goal of this research was to develop biobased nanocomposites through the NC and functionalized NC integration into the epoxy linseed oil (ELO)-based polymeric matrix. This research brought together the advantages of both components through an economically feasible strategy to develop sustainable epoxy−nanocellulose composites for coating applications. The research novelty comes from the original formulations based on renewable raw materials, while maintaining the thermomechanical properties given by a biobased epoxy network crosslinked with a naturally occurring carboxyl-containing compound (citric acid).

■ EXPERIMENTAL SECTION

Materials. The epoxidized linseed oil (ELO) used for the development of the nanocomposites was previously reported in terms of synthesis and characterization.[30] Nanocellulose (NC) obtained from plum seed shells derived from Romanian varieties of plum trees was converted into different functionalized NC samples, which were further used as reinforcing agents. The reagents employed to generate the NC were glacial acetic acid (99.8%) and absolute ethanol (99.5%), which were purchased from Chimreactiv (Bucharest, Romania). Reagent-grade (3-aminopropyl) triethoxysilane (APTS, 99%), (3-glycidyloxypropyl) trimethoxysilane (GPTS, 99%), and high-purity vanillin (V) (Ph.Eur. 0.998%) were purchased from Sigma-Aldrich (Germany) and used for the functionalization of NC. All the reagents and solvents are used in this study without preliminary purification. To crosslink the ELO-based

formulations, citric acid monohydrate (CA, 99.5+%, Alfa Aesar) was used in the presence of anhydrous tetrahydrofuran (THF, ≥99.9%, inhibitor-free, Sigma-Aldrich).

Methods. *Isolation and Modification of NC Structures.* The detailed procedure for the isolation of NC from plum seed shells is reported in a previous study.[31] Briefly, a defined quantity of plum seed shell powder was subjected to successive alkaline and bleaching treatments for the removal of both hemicelluloses and lignin. Acid hydrolysis of the bleached pulp was carried out using 60 wt % H_2SO_4 at 40 °C for 150 min followed by centrifugation to remove the residual acid. Subsequently, the final NC suspension (3 wt % NC) was dialyzed with distilled water until a final pH of ∼7 was attained. For the modification of NC, both silanes, APTS or GPTS, were used at 5 wt % with respect to the ethanol−water solution (90:10 v/v) to obtain OH groups. The silane solution was allowed to hydrolyze for 90 min in acid medium (pH = 4) under continuous stirring. Afterward, the NC water suspension (3 wt % NC) was added to the silane solution (1 mol silane/ mol anhydro glucose unit) and vigorously stirred at ambient temperature for 3 h. The final functionalized NC (denoted as NCA and NCG) was washed and freeze-dried. A part of the NCA was kept in solution for further grafting with vanillin− ethanol solution. A suspension of 4 wt % NCA was obtained in 1:4 wt ratio of vanillin/NCA and stirred for 1 h at room temperature and for another 5 h at 65 °C. The resulting vanillin-grafted NC suspension, denoted as NCV, was purified and then freeze-dried. The functionalization process is schematically represented in Figure 1.

Nanocomposite Synthesis. For the synthesis of ELO-NC nanocomposite systems, the corresponding NC ratios (1, 3, and 5 wt %) were dispersed in the ELO continuous phase for 15 min by using an ultrasonic processor (frequency of 100 KHz and amplitude of 20%). For the curing of the ELO-NC formulations, a 1:1 stoichiometric amount of CA (considering the molar ratio of −COOH groups from the crosslinker and epoxy groups from ELO) was solubilized in THF at 80 °C and then added to the ELO-NC blends. After 5 min of homogenization at 80 °C, the resulting mixtures were placed in Teflon molds and subjected to thermal treatment for 3h at 80 °C, 1 h at 100 °C, and 1 h at 150 °C. Table 1 summarizes the formulated ELO-NC formulations.

Characterization. Fourier transform infrared spectroscopy (FTIR) was used to evaluate the chemical structure of the nanocellulose, and the results were recorded on Bruker Vertex 70 equipment in the 400−4000 cm^{-1} range with 4 cm^{-1} resolution and 32 scans. The samples were analyzed on the attenuated total reflection (ATR) module.

X-ray photoelectron spectrometry (XPS) analysis was performed on a K-Alpha spectrometer with a monochromatic Al Kα source (1486.6 eV) working in a vacuum base pressure of 2×10^{-9} mbar. Charging effects were compensated using a flood gun, and binding energy was calibrated by placing the C 1s peak at 284.8 eV as an internal standard. Deconvolution of C 1s peaks was performed by using a smart background algorithm with a convolved Gaussian−Lorentzian ratio. The pass energy for the survey spectra was set at 200 eV, and it was 20 eV for the high-resolution spectral registration.

Differential scanning calorimetry (DSC) curves were recorded on Netzsch DSC 204 F1Phoenix equipment. The samples were subjected to heating with a rate of 5 °C/min under nitrogen (20 mL/min flow rate) from room temperature (RT) to 300 °C.

Table 1. Composition of ELO-NC Nanocomposites, Components, and Sample Abbreviation

components of the studied systems	
component (filler/polymeric matrix)	component abbreviation
NC	NC
NC-APTS	NCA
NC-GPTS	NCG
NC-vanillin	NCV
ELO matrix	E
ELO-NC nanocomposite formulations			

nanocomposite systems	NC ratio (wt %)	system abbreviation	sample abbreviation
ELO_NCs	1	ENC	ENC1
	3		ENC3
	5		ENC5
ELO_NCs_APTS	1	ENCA	ENCA1
	3		ENCA3
	5		ENCA5
ELO_NCs_GPTS	1	ENCG	ENCG1
	3		ENCG3
	5		ENCG5
ELO_NCs_V	1	ENCV	ENCV1
	3		ENCV3
	5		ENCV5

The thermal properties of the samples were evaluated by thermogravimetric analysis (TGA) by using a Q500 TA Instruments. The analysis was recorded under a nitrogen atmosphere using a heating rate of 10 °C/min from RT to 700 °C.

Dynamic mechanical analysis (DMA) tests were performed on TRITEC 2000 B equipment. Samples were analyzed in the single-cantilever bending mode at 1 Hz frequency from −40 to 100 °C, using a heating rate of 5 °C/min. Based on the DMA, the crosslinking density was calculated with the aid of the following equation

$$v_e = \frac{E'}{3RT} \tag{1}$$

E' = storage modulus at $T = T_g + 30$, R = gas constant, and T = temperature in K corresponding to the storage modulus value.

The surface characteristics were analyzed by contact angle (CA) measurements using a Drop Shape Analyzer-DSA100 from Krüss Scientific GmbH through the static sessile drop method at room temperature by using deionized purified water and ethylene glycol (EG) as reference polar and nonpolar liquids, respectively. The droplet with a volume of 2 μL was maintained on the sample for 5 s. The water contact angle was determined using the Young−Laplace equation in Advance software and represents the average of three measurements for each sample. The determination of surface free energies was performed using the same software, which takes into consideration the Young−Dupré and Fowkes equations.

The degree of water uptake for the epoxy nanocomposite samples was studied according to ASTM 570D. Square samples with 5 mm width side and 2 mm thickness were conditioned for 24 h and weighed using a four-digit balance. The nanocomposites were then immersed in distilled water. Every 24 h, the samples were taken out, and the surfaces were dried with filter papers, weighed, and immediately placed back in the deionized water. The degree of swelling (D_S) was

calculated according to eq 2, where W_0 and W_t are the sample mass of the samples before and after immersing in water for a certain time (t), respectively.

$$D_S = \frac{W_t - W_0}{W_0} \times 100 \qquad (2)$$

Mechanical tests were performed by using a universal mechanical tester Instron, Model 3382, at a relative humidity of 45−50% and a speed of 1 mm/min. The size of the cylindrical samples was approximately 10 × 10 mm^2. A minimum of three specimens were tested for each nano-composite system, and the average values are reported.

The morphology of the functionalized NC-based nano-composites was also analyzed by scanning electron microscopy (SEM). The samples were sputter-coated with gold and investigated using a Quanta 200 Environmental scanning electron microscope (FEI-Philips) with a tungsten electron source, in the low vacuum mode, at an accelerating voltage of 30 kV.

■ RESULTS AND DISCUSSION

Nanocellulose Characterization. The NC used for the synthesis of nanocomposite materials was first characterized in terms of the chemical structure and thermal behavior. FTIR spectrometry provides a structural perspective over the efficiency of each formulated system, by establishing the functional groups from the structure of each type of NC, which were used to obtain the nanocomposite formulations. The FTIR spectra for pristine NC and its functionalized derivatives are presented in Figure 2, comprising the main characteristic
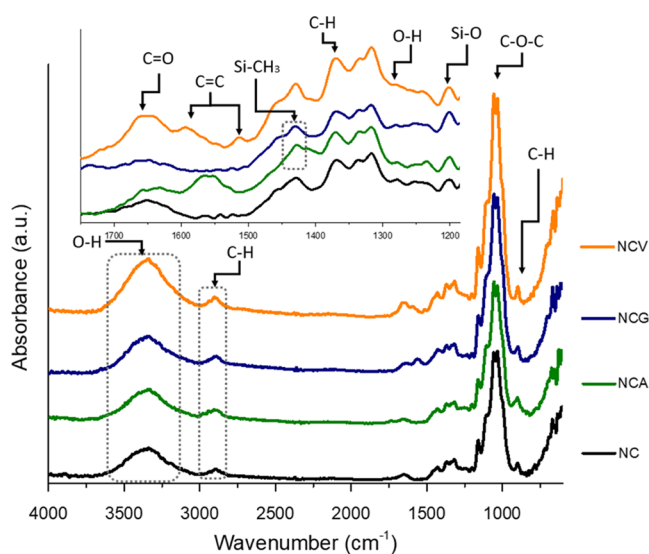

Figure 2. FTIR spectra for neat NC and chemically functionalized NC. Inset: zoomed spectral range of 1200−1700 cm^{-1}.

peaks according to their structure. The absorption bands corresponding to the cellulose backbone are observed: the peak at ∼3350 cm^{-1} is attributed to the OH stretching vibrations, the one at ∼2897 cm^{-1} corresponds to the C−H stretching vibrations,[32] the peak at ∼1650 cm^{-1} is assigned to the O−H stretching from the absorbed water,[33] and then, the following peaks from the polysaccharide ring vibration of C−H and C−O are registered at 1320−1370 cm^{-1}. The character-istic etheric bonds that build the structural unit of the NC are

represented by the C−O−C vibration signal at ∼1053 cm^{-1} and C−H stretching vibrations from ∼1365 cm^{-1}.[34] These signals are present in all recorded spectra. Apart from these aspects, the spectra of silane-treated NC structures (NCA and NCG) show absorption signals at ∼1150 and ∼1202 cm^{-1} related with −Si−O−Si− linkage and −Si−O−C bonds masked by the large and intense polysaccharide C−O−C vibrations, respectively.[23] The successful chemical linkage of the APTS molecule over the NC macromolecular chain is also confirmed first by a new shoulder observed at 2938 cm^{-1} in NCA, which is characteristic of the C−H stretching vibration in the propyl moiety of the asymmetric vibration in CH$_2$ at 2929 cm^{-1}[15] and then by the amide band at 1560 cm^{-1}, thus proving the functionalization reaction[35] and the efficiency of the NC surface compatibilization with the bioepoxy matrix derived from ELO.

In the case of NCV structures, a functionalization strategy with two possible resulting structures was proposed[36] as depicted in Figure 1, a Schiff base linkage between NH$_2$ and the attached APTS or an acetalization of OH groups from the NC backbone. Thus, based on the presence of the C=C stretching vibration peak at 1516 cm^{-1} and the shoulder from the C=O vibration at 1733 cm^{-1}, the second structure is prevailing.

X-ray Photoelectron Spectroscopy (XPS). The XPS analysis provides valuable information regarding the surface elemental analysis by determining the specific atomic bands of the constituent electrons in the analyzed samples. Thus, from the general spectra of NC structures (Figure 3), one can observe
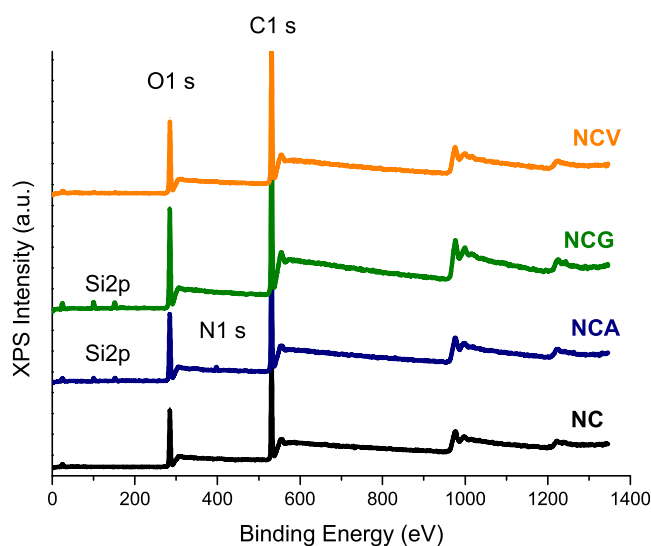

Figure 3. Surface elemental analysis of the NC-based nanomaterials by XPS survey.

the presence of the main bands assigned to C 1s located at 284.8 eV and O1s from 531 eV. For NCA, surface analysis showed two new peaks at 101 eV assigned to Si 2p species with one at 399 eV for N 1s species. The composition at the NCA surface revealed 2.98% at. Si 2p species, simultaneously with 2.25% at. N1s species following the functionalization with APTS.[37] Similarly, the functionalization with GPTS is highlighted with the presence of 4.3% at. Si 2p coming from the silane structure. The attachment of vanillin is difficult to assign through surface composition; however, it can be determined by indirect methods, like the calculation of the
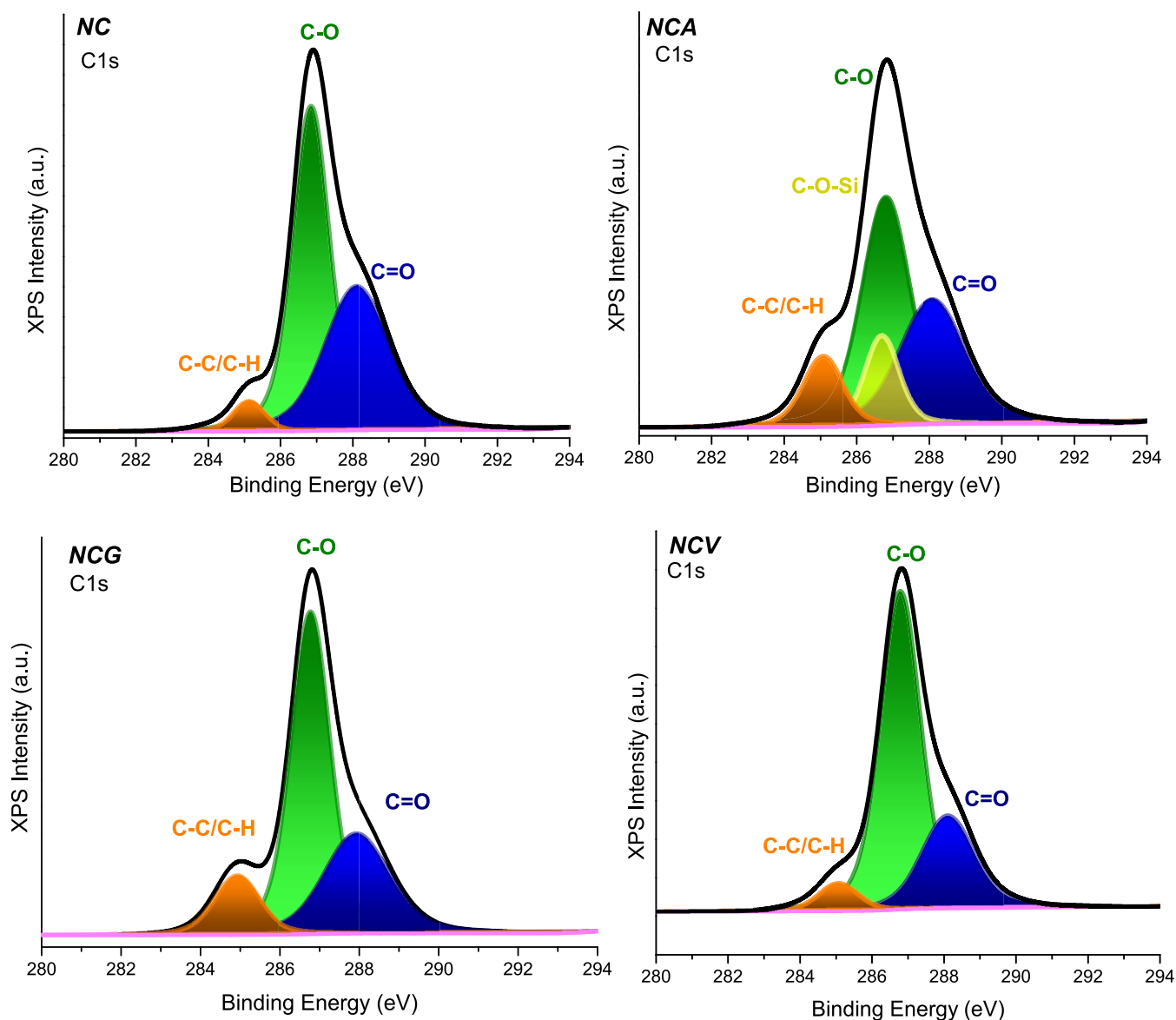
Figure 4. High-resolution C1s spectral deconvolution from XPS of neat NC and chemically functionalized NC.

C/O atomic ratio. Thus, its value was noticed to change from 0.552 corresponding to NCs to 0.532 computed for NCV.[38]

The deconvolution of the high-resolution XPS spectra for NCs (Figure 4) reveals the presence of secondary bands attributed to electronic species involved in different bonds like C–C/C–H obtained at 284.8 eV, C–O which appeared at 286.2 eV, or the band attributed to C=O from 288.4 eV.[39] The main contribution comes from the C–O species, in accordance with the NC structure. After performing the functionalization reaction on the NC structure, the C 1s spectrum of NCA is modified first if C–O to C–C/C–H ratio is considered and second by the appearance of a new secondary peak assigned to C–O–Si at 286.7 eV. In the case of NCA and NCV in the deconvolution of high-resolution XPS spectra of C1s, the C–N secondary peak overlaps with the C–O one; thus, it is difficult to assess.[40]

Thermogravimetric Analysis (TGA). The chemical modifications performed on NC can also be demonstrated with the aid of thermal analysis.[41] Thermal decomposition of the NC structures was assessed through TGA, with the curves shown

in Figure 5 corresponding to the numerical values shown in Table 2. The results revealed that all the functionalized NC derivatives are more thermally stable in the first stage of degradation than the nonfunctionalized NC, registering higher $T_{d3\%}$ values assigned to an initial absorbed water loss. Then, as the temperature increases, the rank of thermal stability changes; however, it can be seen that NC functionalized with vanillin registers the highest thermal stability, over the studied temperature regime. This behavior can be attributed to the aromatic nucleus in the vanillin structure, which induces a superior thermal stability to this derivative along with the possibility of being described as an alternative functionalization route for acetal NCV structure formation in Figure 1. Another hypothesis which arises is that of NC network formation by H bonding, and in this context, NCV stands out for the highest temperature for the discussed parameter ($T_{d3-10\%}$ increased by more than 60 °C).

The inset DTG profiles show the maximum decomposition temperature assigned for the modifier agent attached to the NC surface along with the pyranose rings from the backbone.
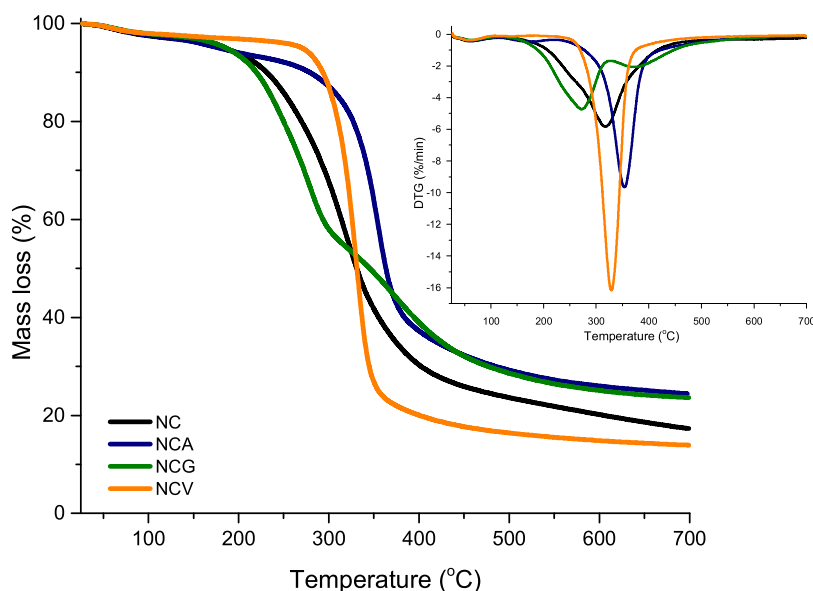
Figure 5. TGA curves and DTG profiles (inset) of neat NC and chemically functionalized NC.

Table 2. Thermal Characteristics from TGA for the Degradation of NC Type Structures

sample	$T_{d3\%}$ (°C)	$T_{d5\%}$ (°C)	$T_{d10\%}$ (°C)	T_{max} (°C) from DTG	residual mass (%)
NC	121.8	183.5	231.4	318.8	17.30
NCA	127.3	177.7	278.9	354.9	24.40
NCG	148.7	186.1	219.8	277.2	23.60
NCV	184.5	270.4	293.5	330.1	13.91

Thus, the most thermally labile sample seems to be GPTS, while APTS degrades at the highest temperature. The data for the residual mass observed for modified NCs are consistent with the functionalization mechanism in which the presence of both APTS and V on the NCV structure can give the highest functionalization degree. In the case of the silane-modified NCs, the resultant undecomposed silicon will influence the final residual mass, giving a higher value.

Nanocomposite Characterization. *Differential Scanning Calorimetry (DSC).* To monitor the crosslinking reaction, DSC analysis was performed for the systems formulated based on ELO and NC derivatives. As can be seen from the curves shown in Figure 6, regardless of the type of NC used for the bio-nanocomposite synthesis, a single maximum is recorded for the crosslinking reactions of the developed systems. According to literature data,[42] higher reaction temperatures (150 °C) can facilitate the formation of β-hydroxyester bonds generated by the reaction between the epoxy rings and the carboxylic groups in the citric acid used for crosslinking.[43] These links can give the bio-nanocomposites unique properties in terms of self-repair, relaxation, and/or covalent crosslinking capacity. In general, when the reinforcing agent is added, there is a decrease in the reactivity of the system, except for the system with NCG, where the excess of epoxy groups on the nanocellulose surface has a slight catalytic effect. The value of the enthalpy of the crosslinking reaction (Table 3), calculated as the area of the curve corresponding to the sample from $t = 0$ in the reaction between ENC and E, decreases. This behavior can be explained by a steric hindrance mechanism given by the reinforcement structures, influencing the mobility of the fatty acid chains contained in ELO and,

consequently, the movement of the citric acid molecules for the formation of reaction centers in order to obtain the epoxy polymer network.

From the data obtained following the DSC characterization, a clear bridge cannot be established between the NC content and the reactivity of the ENC systems in the crosslinking processes, due to (i) the complexity of the formulated systems, (ii) the ELO molecules, with three alternatives related to the epoxidized fatty acids and the multiple possibilities associated with the distribution of epoxy rings on these chains, (iii) the large number of functional groups which are present in the system and from here the multiple reaction possibilities, and (iv) the variable degree of flexibility of the molecules in the formulated systems.

Dynamic Mechanical Analysis (DMA). To study the influence of the different types of functionalized NCs over the thermomechanical properties of ENC systems, the variation of the storage modulus (E') and tan δ values was evaluated by DMA analysis. This technique provides valuable information regarding the stiffness of the polymers as well as the relaxations of the molecular chains. Figure 7 shows the curves of the storage modulus (E') and tan δ as a function of temperature for the synthesized ENC nanocomposite systems, and the correlated parameters such as T_g values and crosslinking density are presented in Table 3. Analyzing the DMA graphs (Figure 6), one can observe that compared to each nanocomposite system, the E matrix registers superior mechanical properties and a higher T_g value.

The broad allure of the tan δ peak is a result of the wide distribution of the molar mass of the epoxidized linseed oil,[44] which is susceptible to chain fragmentation during the ultrasonication process involved in the nanofiller dispersion within the matrix.[45] In the case of each nanocomposite system, the broadening of the tan δ peak can be observed, along with irregular variations of the T_g. T_g is a parameter related with the mobility of the macromolecular chains, and thus, in the case of nanocomposite materials, the nanofiller disrupts the integrity of the organic phase and also restricts the mobility of the vicinal segments. On another note, this phenomenon denotes
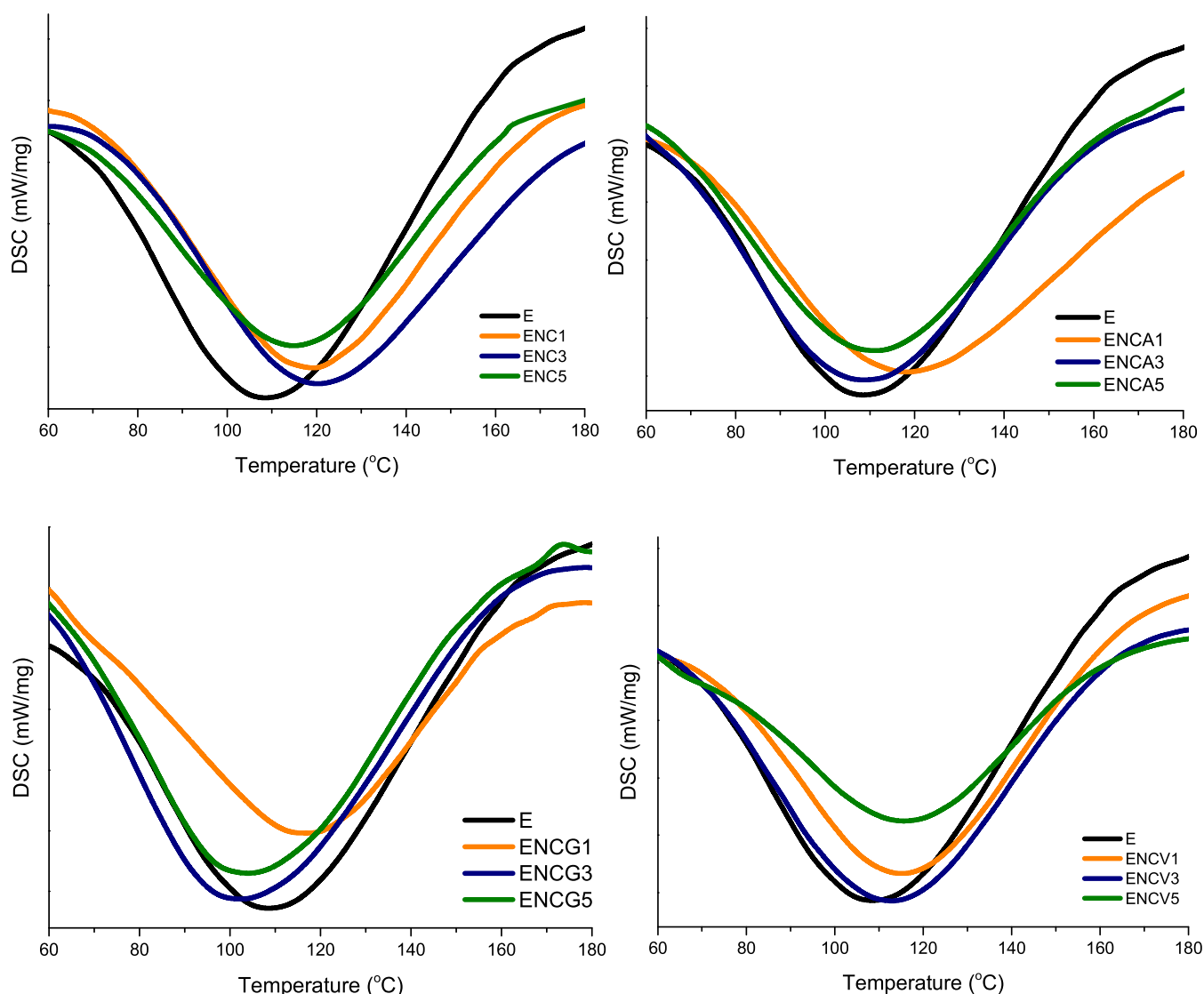
Figure 6. DSC curves registered for the ELO-NC formulation curing process.

Table 3. Thermal Features for ELO-NC Type Nanocomposites

sample	NC ratio (%)	T_g (°C)[a]	crosslinking density (mol/cm³)[a]	ΔH (J/g)[b]	T_{max}[b]	D_S (%)[c]
E		45.2	1393	174.1	108.0	32.8
ENC	1	34.4	2550	152.3	119.3	6.6
	3	37.0	1324	148.3	120.3	7.1
	5	21.2	1384	117.8	114.9	9.7
ENCA	1	31.1	2410	162.4	118.3	7.1
	3	38.9	2206	187.8	108.5	9.3
	5	39.4	1864	176.6	111.3	5.3
ENCG	1	21.5	776	145.7	116.7	9.8
	3	18.1	982	195.4	102.3	7.8
	5	17.7	464	216.0	104.2	6.4
ENCV	1	25.7	899	154.3	115.1	6.5
	3	25.4	552	172.4	112.9	5.4
	5	27.3	951	116.2	115.7	6.2

[a]From DMA data. [b]From DSC data. [c]From water uptake.

an increased interaction between the dispersed phase and the polymeric matrix.[46,47]

The thermomechanical behavior reflected by the T_g values of the nanocomposite systems is dependent on the morphology of the reinforcement agents used in each case. The T_g values for ENCV and ENCA register a slight increase, while in the case of ENC and ENCG nanocomposites, a slight decrease was observed. This behavior is attributed to the nanocellulose that due to its bulky molecules can act as restricting points for the mobility of the macromolecular chains, and therefore, higher temperatures are required to provide the thermal energy required to cause a glass transition. At the same time, the presence of NC can have a negative influence on the crosslinking process, an effect associated with the large specific surface that will lead to the steric hindrance of the reactive groups and, consequently, to a lower crosslinking density.

The crosslinking density represents an important parameter in the characterization of thermorigid materials, which was determined with the help of eq 1, registered for the final cured ELO-NC-type materials. The corresponding values are presented in Table 3. The decrease in crosslinking density values as a result of the increase in the concentration of NC supports the previously formulated hypothesis regarding the
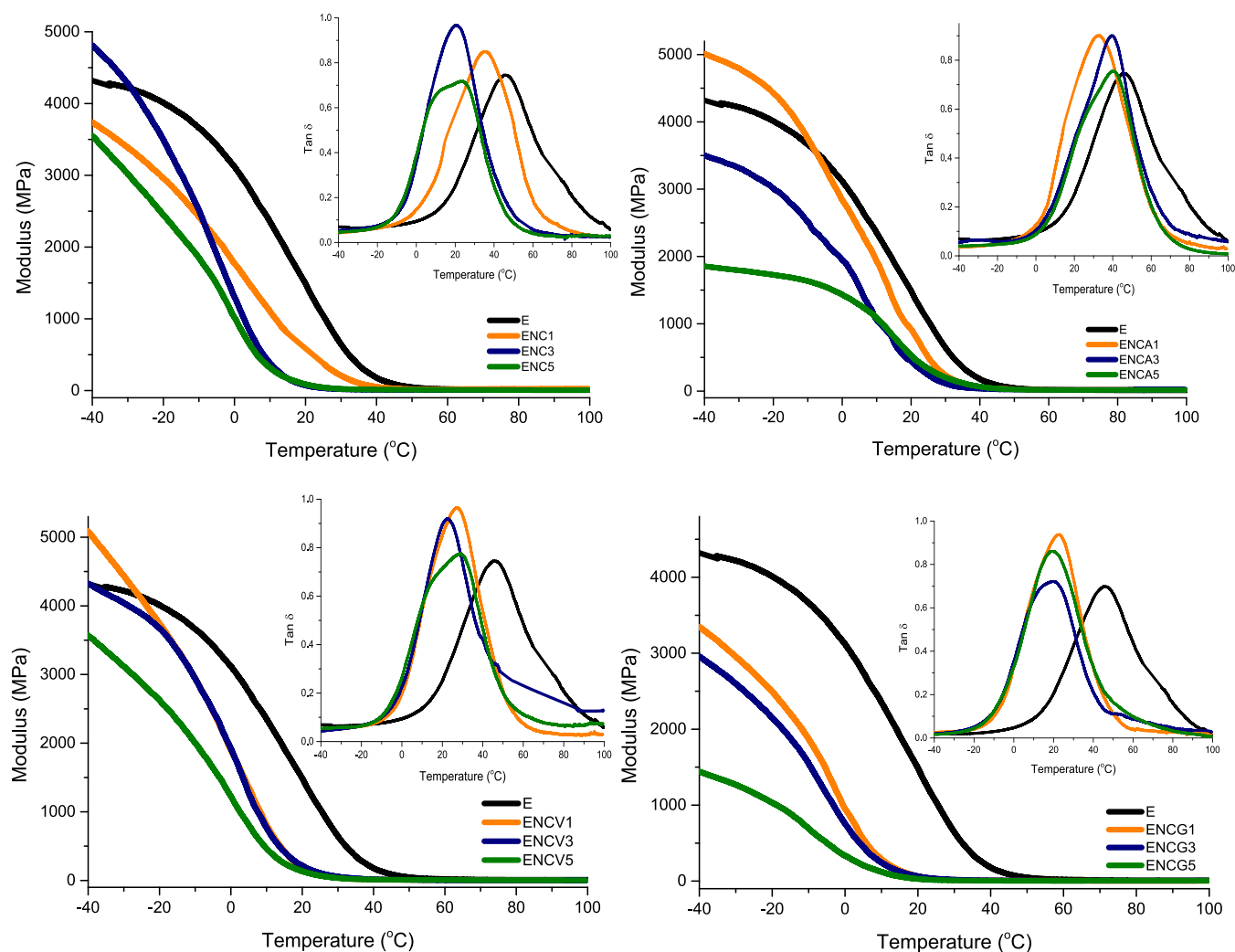
Figure 7. Graphical representation for storage modulus and tan δ (inset) curves for ENC nanocomposites.

restriction of the mobility of the molecular chains. The superior values for the network density determined in the case of ENCA indicate a better compatibility of the silane-treated NC with the ELO polymer matrix. As expected, in the case of 5% nanocomposite formulations, the lower crosslinking density came from the tendency of the NC to form agglomerates, which consequently induce structural defects.

Water uptake properties are important features of biobased epoxy nanocomposites since the applications considered for the newly developed materials should be in the coating industry. Thus, the degree of swelling (D_S) at equilibrium was determined, and the results are included in Table 3. Experimental data of D_S clearly show that the ELO-NC nanocomposites had similar water uptake properties regardless of the surface modifier attached to NC nanostructures; however, the vanillin molecules are impeding water molecule penetration within the nanocomposite network, probably due to the acetal structure formation along with a partial NC network connection, which is consistent with the statement issued after FTIR and TGA results. For the neat ELO network, the high value observed for D_S could be caused by the OH groups formed upon the oxirane ring opening during the crosslinking process, while for the bio-nanocomposites, these groups could be blocked by H bonding with the NC structures.[48]

Thermogravimetric Analysis (TGA). Regarding the thermal stability of the ENC materials, thermal degradation profiles were recorded, and the results are presented in Figure 8. As it can be seen from the TGA and DTG curves of the nanocomposites, the first degradation transition occurred between 200 and 300 °C. This is a consequence of the presence of nanocellulose that has multiple functionalities along with absorbed water.[49] However, this transition is not present in the E matrix due to the nonpolar nature of the monomer that cannot absorb water. The main degradation step occurs in all thermograms between 300 and 500 °C and is assigned to the degradation and pyrolysis of the epoxy macromolecule backbone along with the cleavage of the glycosidic bonds.[50]

Nevertheless, the thermal properties show a decrease for all nanocomposite materials studied, compared to the vegetable oil-derived matrix. This behavior can be explained by the percolation threshold effect, which consists in reaching a maximum level of reinforcement in nanocomposites, above which, even after the functionalization of NC, agglomerations result in the polymer matrix.[51] On the other hand, it is possible that through functionalization, the compatibility of NC with the continuous phase of ELO is still improved, but the presence of the newly grafted functional groups on the surface of NC (derived from APTS, GPTS, V) leads to a decrease in
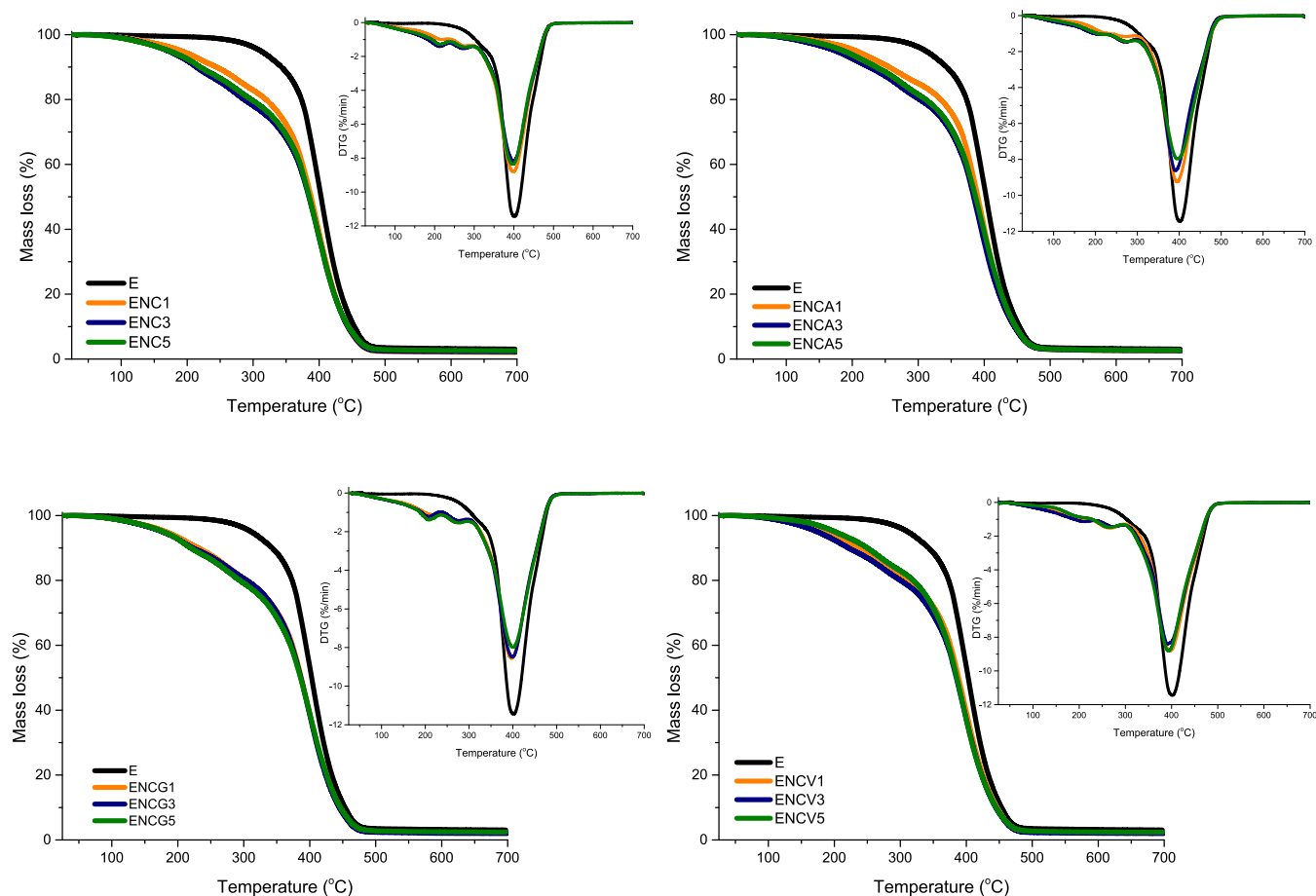
Figure 8. TGA profiles for ENC nanocomposite materials.

the general thermostability of each composite material studied, their chemical bonds being easily split under the influence of temperature.

However, compared to the ENC systems, those with the functionalized NC showed improved thermal properties, regardless of the proportion in which the reinforcing agent is added. Also, the ENCV materials stand out by recording the highest stability in the studied temperature range, compared to the nanocomposites with nonfunctionalized NC, this characteristic being reflected by the $T_{d3\%}$ values (Table 4). This may be a consequence of the aromatic decoration of NC through vanillin functionalization.

It is widely known that in the first stage of thermal degradation, the small molecular fractions are decomposed. Thus, the reduced thermal stability of the functionalized NC can be a consequence of this aspect. T_{max} represents the temperature at which the degradation of the materials reaches the highest rate, and the values calculated from the derivative of the thermogravimetric curves (Figure 8) are not dramatically influenced by the presence of NC derivatives in the vegetable oil matrix; the range of differences is within a range of 10 °C.

Surface Characteristics. Surface water affinity was also evaluated for the studied nanocomposites, and the results are depicted in Figure 9. The surface characteristics are important parameters in the case of epoxy resins, which mainly have an adhesive role. The polar character of the NC derivatives, conferred by the numerous −OH groups, has significant consequences on the hydrophilic character of the synthesized

Table 4. Thermal Parameters Determined from TGA for the Studied ELO-NC Type Nanocomposites

sample	NC ratio (%)	$T_{d3\%}$ (°C)	T_{max} (°C) from DTG	residual mass (%)
E		290.3	401.7	3.07
ENC	1	158.3	399.5	2.02
	3	143.4	398.3	2.23
	5	142.2	396.0	2.56
ENCA	1	174.8	394.6	2.44
	3	143.6	390.1	2.58
	5	157.4	394.8	2.67
ENCG	1	150.9	397.3	2.12
	3	146.8	398.9	1.97
	5	149.2	399.6	2.43
ENCV	1	161.6	396.4	2.20
	3	146.9	391.5	1.99
	5	175.2	392.9	2.38

materials. Thus, naturally, due to its more hydrophilic character, a decrease in CA values is observed for materials with the NC content, regardless of the derivatization molecule, compared to the ELO reference system, with an accentuated hydrophobic character, due to the chemical nature of the epoxy derivative (vegetable oil). It is also observed that small additions (1%) of NC and NCV do not produce considerable variations in the hydrophobicity of the surface of the materials, compared to the ELO reference matrix, and in the case of NC, a decrease in CA values is noted with increasing additive content. The ENCV material with 5% content of the cellulosic
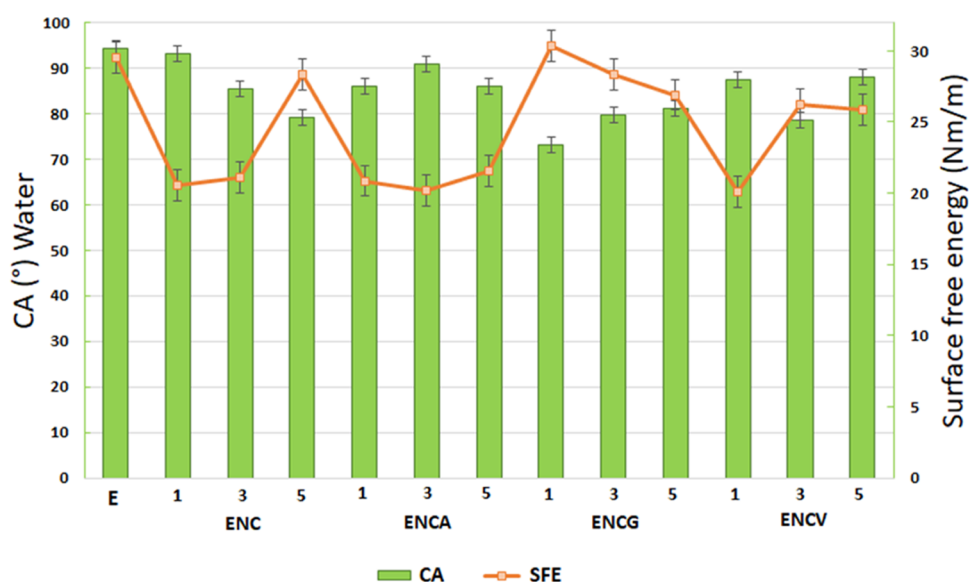
Figure 9. Surface characteristics for ELO-NC nanocomposite materials.

derivative records the same CA value as the one with 1% content, although the values are quite close to those recorded by the reference system (ELO). The presence of the aromatic vanillin structure is thus noted, which does not dramatically influence the hydrophobicity of the matrix derived from vegetable oil.

For the ENCA and ENCG nanocomposites, no relationship can be established between the variation of the hydrophilic character and the functionalized NC additive content.

The surface free energy can give an estimate of the adhesion of the bio-nanocomposite to different types of substrates, in order to be used as protective coatings in electronics. Although the reference value (43 mJ/m^2) for coatings based on conventional epoxy matrices is higher than the value of the surface free energy of the developed bio-nanocomposites developed, it must be taken into account that one of the most important factors in determining the resistance to adhesion is if the surface energy of the substrate is close to or greater than the surface energy of the crosslinked coating material. The surface free energy value for E networks is in the range with the substrates with low surface energy, such as silicon, a material often used in electronics. Therefore, the application of flexible coatings considered is of interest in the electronics industry.

Mechanical Tests. The mechanical properties of the studied ENC nanocomposites were evaluated by performing mechanical compression tests on cylindrical specimens as part of the visioned applications as encapsulation materials for electronic devices or coatings. In this area, the contribution given by the presence of NC structures is already established, according to Karki;[52] the bio-nanocomposites developed in this study can benefit from the low dynamic loss and high sonic velocity properties of NC, besides being a source of reinforcement. From Table 5, it can be seen that the use of 1 and 3% NC led to a notable effect on increasing the modulus of elasticity and thus the compressive strength of ENC materials; however, the 5% content of NC improved only the compressive strength, probably due to an agglomeration effect. As observed from the DSC and DMA data, for the NC-based nanocomposites, a low crosslinking enthalpy and a degree of crosslinking similar to the matrix suggest that the stiffness of the nanocomposite may

Table 5. Mechanical Parameters of ENC Nanocomposite Materials

sample	NC ratio (%)	*E* (MPa)	compressive strength (MPa)
E		5.08	18.50
ENC	1	5.50	135.22
	3	7.07	89.42
	5	3.60	38.60
ENCA	1	1.71	12.18
	3	1.47	16.67
	5	1.20	39.99
ENCG	1	0.30	14.89
	3	0.84	11.60
	5	0.90	9.46
ENCV	1	2.89	129.04
	3	6.80	56.95
	5	3.27	17.40

come from the agglomerated nanostructures due to the low compatibility with the epoxy matrix.

In the case of the vanillin NC derivative, the creation of C−O−C bridges through the acetalization reaction conducted on a nanocellulose network simultaneously with the introduction of rigid benzene rings can be the logical conclusion in increasing the stiffness of the nanocomposite with a percentage of 3%, after which the agglomeration effects interpose by reaching the maximum of the reinforcing effect. However, with the increase in the content of the NC derivative, the compressive strength decreases. This behavior can be explained by the reduced compatibility between NC derivatives and the phase derived from vegetable oil, an effect that is accentuated with the increase of the amount of additive in the continuous phase of E.

The ENCA and ENCG composites show low mechanical compressive strength regardless of the NC content used. In the case of APTS-modified NC structures, a possible explanation could be the plasticizing effect of silane molecules involved within the ELO network, as suggested by the higher crosslinking density value and the enthalpy of the reaction. In the case of oxirane groups from the GPTS, the effect exerted
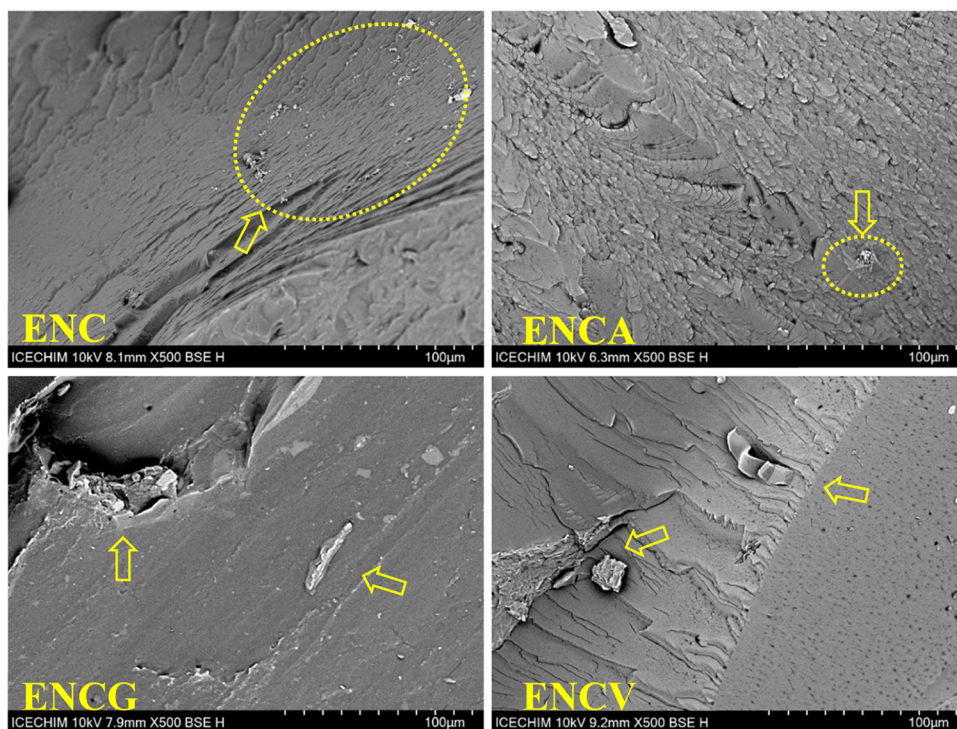
Figure 10. SEM micrographs for ELO nanocomposites with 3% nanocellulose.

could be as hindering points in the crosslinking process, as a lower crosslinking density from DMA results suggests.

The deformation capacity of the nanocomposites reinforced with NC and derivatives functionalized based on NCs presents values between 1.4 and 2. This deformation range can be comparable to formulations of coatings based on conventional epoxy resins.[53]

Scanning Electron Microscopy (SEM). The morphological analysis of the studied nanocomposites indicates the presence of agglomerations of NC derivatives in the ELO polymer matrix, regardless of the functionalization agent used (Figure 10); this behavior is in accordance with similar studies, which showed that the NC structure forms aggregates due to the high surface energy of the nanoparticles.[26] Also, a slightly smoother architecture is noted in the case of the ENC composite, while the composites with the functionalized NC present a rougher appearance, probably due to the grafted agents on the structure of the nanocellulose derivatives, which increase the interphase volume and thus the compatibility with the bioepoxy network. By analyzing the morphology of the fracture, one can observe that in each case, the particle distribution within the matrix varies as a consequence of the functionalization agent used as an interface generator. The nanocomposite with the unmodified nanocellulose reveals an agglomeration at the surface of the fracture due to the presence of hydrophilic OH groups from its structure, while in the case of the silane-functionalized nanocellulose (NCA), these groups are transformed into a more compatible interface with the ELO matrix. The particles evidenced in the SEM micrograph of ENCA suggest a better compatibility with the polymeric matrix as previously demonstrated by the DMA results. The ENCG nanocomposite also displays a good compatibility between the two components by revealing nanoparticle fragments entrapped in the polymeric matrix after the breaking of the sample.

CONCLUSIONS

Sustainable epoxy networks reinforced with different functionalized NC structures were successfully synthesized as alternative green materials to meet specific application requirements for the anticorrosion coating industry. APTS functionalization of NC structures greatly improved the compatibility with the ELO-type matrix, as it was observed from a crosslinking degree value over 2400 mol/cm^3 of ELO networks, increased roughness features in the SEM micrographs, and water uptake decrease at the same time, showing a contact angle value close to that of the hydrophobic domain; these are the key assets of the developed sustainable nanocomposites. The thermomechanical results suggest a great influence exerted by the silane functional groups attached to the NC structures in the case of the storage modulus of the ELO nanocomposite: in the glassy state, only a ratio of 1% NCA increased the storage modulus by 20%. A similar increase in the storage modulus was noticed also for the addition of 3% NC.

AUTHOR INFORMATION

Corresponding Author

Celina M. Damian − *Advanced Polymer Materials Group, University Politehnica of Bucharest, 011061 Bucharest, Romania;* ⊙ orcid.org/0000-0001-6109-6630; Email: celina.damian@upb.ro

Authors

Mădălina I. Necolau − *Advanced Polymer Materials Group, University Politehnica of Bucharest, 011061 Bucharest, Romania*

Brîndușa Bălănucă − *Advanced Polymer Materials Group, University Politehnica of Bucharest, 011061 Bucharest, Romania; Department of Organic Chemistry "C. Nenitescu",*

University Politehnica of Bucharest, 011061 Bucharest, Romania

Adriana N. Frone − *National Institute for Research & Development in Chemistry and Petrochemistry-ICECHIM, 060021 Bucharest, Romania;* ⊙ orcid.org/0000-0001-6232-886X

Complete contact information is available at:
https://pubs.acs.org/10.1021/acsomega.2c07033

Notes
The authors declare no competing financial interest.

■ REFERENCES

(1) Yang, J.; Dong, X.; Wang, J.; Ching, Y. C.; Liu, J.; Chunhui, l.; Baikeli, Y.; li, Z.; Mohammed Al-Hada, N.; Xu, S. Synthesis and properties of bioplastics from corn starch and citric acid-epoxidized soybean oil oligomers. *J. Mater. Res. Technol.* **2022**, *20*, 373−380.

(2) He, W.; Huang, H.; Xie, L.; Wang, C.; Yu, J.; Lu, S.; Fan, H. The influence of self-crosslinked epoxidized castor oil on the properties of Poly (lactic acid) via dynamic vulcanization: Toughening effect, thermal properties and structures. *Colloids Surf., A* **2021**, *630*, No. 127517.

(3) Petrović, Z. S.; Hong, J.; Vuković, M. L.; Djonlagić, J. Epoxy resins and composites from epoxidized linseed oil copolymers with cyclohexene oxide. *Biocatal. Agric. Biotechnol.* **2022**, *39*, No. 102269.

(4) Kumar, S.; Ngasainao, M. R.; Sharma, D.; Sengar, M.; Gahlot, A. P. S.; Shukla, S.; Kumari, P. Contemporary nanocellulose-composites: A new paradigm for sensing applications. *Carbohydr. Polym.* **2022**, *298*, No. 120052.

(5) Zulaikha, W.; Hassan, M. Z.; Ismail, Z. Recent development of natural fibre for nanocellulose extraction and application. *Mater. Today: Proc.* **2022**, *66*, 2265−2273.

(6) Ma, T.; Hu, X.; Lu, S.; Liao, X.; Song, Y.; Hu, X. Nanocellulose: a promising green treasure from food wastes to available food materials. *Crit. Rev. Food Sci. Nutr.* **2022**, *62*, 989−1002.

(7) Kamel, R.; El-Wakil, N. A.; Dufresne, A.; Elkasabgy, N. A. Nanocellulose: From an agricultural waste to a valuable pharmaceutical ingredient. *Int. J. Biol. Macromol.* **2020**, *163*, 1579−1590.

(8) Xu, T.; Du, H.; Liu, H.; Liu, W.; Zhang, X.; Si, C.; Liu, P.; Zhang, K. Advanced Nanocellulose-Based Composites for Flexible Functional Energy Storage Devices. *Adv. Mater.* **2021**, *33*, No. 2101368.

(9) Zhu, L.; Feng, L.; Luo, H.; Dong, R.-s.; Wang, M.-y.; Yao, G.; Chen, J. Characterization of polyvinyl alcohol-nanocellulose composite film and its release effect on tetracycline hydrochloride. *Ind Crops Prod.* **2022**, *188*, No. 115723.

(10) Zhou, Y.; Wang, F.; Yang, Z.; Hu, X.; Pan, Y.; Lu, Y.; Jiang, M. 3D printing of polyurethane/nanocellulose shape memory composites with tunable glass transition temperature. *Ind. Crops Prod.* **2022**, *182*, No. 114831.

(11) Jabbar, A.; Militký, J.; Wiener, J.; Kale, B. M.; Ali, U.; Rwawiire, S. Nanocellulose coated woven jute/green epoxy composites: Characterization of mechanical and dynamic mechanical behavior. *Compos. Struct.* **2017**, *161*, 340−349.

(12) Meng, X.; Bocharova, V.; Tekinalp, H.; Cheng, S.; Kisliuk, A.; Sokolov, A. P.; Kunc, V.; Peter, W. H.; Ozcan, S. Toughening of nanocelluose/PLA composites via bio-epoxy interaction: Mechanistic study. *Mater. Des.* **2018**, *139*, 188−197.

(13) Noguchi, T.; Niihara, K.-i.; Iwamoto, R.; Matsuda, G.-i.; Endo, M.; Isogai, A. Nanocellulose/polyethylene nanocomposite sheets prepared from an oven-dried nanocellulose by elastic kneading. *Compos. Sci. Technol.* **2021**, *207*, No. 108734.

(14) Bonini, C.; Heux, L.; Cavaillé, J.-Y. Polypropylene reinforced with cellulose whiskers. *Mater. Tech.* **2000**, *88*, 55−58.

(15) Mani, S.; Graceraj, P., Nanocellulose Based Plastics and Composites, 2022.

(16) Masek, A.; Kosmalska, A. Technological limitations in obtaining and using cellulose biocomposites. *Front. Bioeng. Biotechnol.* **2022**, *10*, No. 912052.

(17) Patanair, B.; Saiter-Fourcin, A.; Thomas, S.; Thomas, M. G.; Pundarikashan, P. P.; Gopalan Nair, K.; Kumar, V. K.; Maria, H. J.; Delpouve, N. Promoting Interfacial Interactions with the Addition of Lignin in Poly(Lactic Acid) Hybrid Nanocomposites. *Polymers* **2021**, *13*, No. 272.

(18) Guo, Q.; Zhu, P.; Li, G.; Wen, J.; Wang, T.; Lu, D.; Sun, R.; Wong, C. Study on the effects of interfacial interaction on the rheological and thermal performance of silica nanoparticles reinforced epoxy nanocomposites. *Composites, Part B* **2017**, *116*, 388−397.

(19) Hu, D.; Liu, H.; Ding, Y.; Ma, W. Synergetic integration of thermal conductivity and flame resistance in nacre-like nanocellulose composites. *Carbohydr. Polym.* **2021**, *264*, No. 118058.

(20) Yu, T.; Soomro, S. A.; Huang, F.; Wei, W.; Wang, B.; Zhou, Z.; Hui, D. Naturally or artificially constructed nanocellulose architectures for epoxy composites: A review. *Nanotechnol. Rev.* **2020**, *9*, 1643−1659.

(21) Kaur, P.; Sharma, N.; Munagala, M.; Rajkhowa, R.; Aallardyce, B.; Shastri, Y.; Agrawal, R. Nanocellulose: Resources, Physio-Chemical Properties, Current Uses and Future Applications. *Front. Nanotechnol.* **2021**, *3*, No. 747329.

(22) Vinothkumar, M.; Sasikumar, M. Silane Grafted Cellulose and Biosilica Toughened Glass-Epoxy Composite: Mechanical, Hydrophobicity and Low Velocity Impact Behavior. *Silicon* **2022**, *14*, 3601−3613.

(23) Yamato, K.; Yoshida, Y.; Kumamoto, Y.; Isogai, A. Surface modification of TEMPO-oxidized cellulose nanofibers, and properties of their acrylate and epoxy resin composite films. *Cellulose* **2022**, *29*, 2839−2853.

(24) Thompson, L.; Nikzad, M.; Sbarski, I.; Yu, A. Esterified cellulose nanocrystals for reinforced epoxy nanocomposites. *Prog. Nat. Sci.: Mater. Int.* **2022**, *32*, 328−333.

(25) Pacaphol, K.; Aht-Ong, D. The influences of silanes on interfacial adhesion and surface properties of nanocellulose film coating on glass and aluminum substrates. *Surf. Coat. Technol.* **2017**, *320*, 70−81.

(26) Roszowska-Jarosz, M.; Masiewicz, J.; Kostrzewa, M.; Kucharczyk, W.; Żurowski, W.; Kucińska-Lipka, J.; Przybyłek, P. Mechanical Properties of Bio-Composites Based on Epoxy Resin and Nanocellulose Fibres. *Materials* **2021**, *14*, No. 3576.

(27) Kuo, P.-Y.; Barros, L. d. A.; Yan, N.; Sain, M.; Qing, Y.; Wu, Y. Nanocellulose composites with enhanced interfacial compatibility and mechanical properties using a hybrid-toughened epoxy matrix. *Carbohydr. Polym.* **2017**, *177*, 249−257.

(28) Wang, H.; Wu, J.; Huang, B.; Lu, Q.-L. One-Pot Synthesis of UPy-Functionalized Nanocellulose under Mechanochemical Synergy for High-Performance Epoxy Nanocomposites. *Polymers* **2022**, *14*, No. 2428.

(29) Wang, B.; Zhou, J.; Wang, Z.; Mu, S.; Wu, R.; Wang, Z. Cellulose nanocrystal/plant oil polymer composites with hydrophobicity, humidity-sensitivity, and high wet strength. *Carbohydr. Polym.* **2020**, *231*, No. 115739.

(30) Necolau, M. I.; Damian, C. M.; Olaret, E.; Iovu, H.; Balanuca, B. Comparative Thermo-Mechanical Properties of Sustainable Epoxy Polymer Networks Derived from Linseed Oil. *Polymers* **2022**, *14*, No. 4212.

(31) Frone, A. N.; Batalu, D.; Chiulan, I.; Oprea, M.; Gabor, A. R.; Nicolae, C.-A.; Raditoiu, V.; Trusca, R.; Panaitescu, D. M. Morpho-Structural, Thermal and Mechanical Properties of PLA/PHB/Cellulose Biodegradable Nanocomposites Obtained by Compression Molding, Extrusion, and 3D Printing. *Nanomaterials* **2020**, *10*, No. 51.

(32) Wulandari, W. T.; Rochliadi, A.; Arcana, I. M. Nanocellulose prepared by acid hydrolysis of isolated cellulose from sugarcane bagasse. *IOP Conf. Ser.: Mater. Sci. Eng.* **2016**, *107*, No. 012045.

(33) Mandal, A.; Chakrabarty, D. Isolation of nanocellulose from waste sugarcane bagasse (SCB) and its characterization. *Carbohydr. Polym.* **2011**, *86*, 1291−1299.

(34) Nuruddin, M.; Hosur, M.; Mahdi, T.; Jeelani, S. Flexural, Viscoelastic and Thermal Properties of Epoxy Polymer Composites Modified with Cellulose Nanofibers Extracted from Wheat Straw. *Sens. Transducers* **2017**, *210*, 1−8.

(35) Alanis, A.; Valdés, J. H.; Guadalupe, N.-V. M.; Lopez, R.; Mendoza, R.; Mathew, A. P.; de León, R. D.; Valencia, L. Plasma surface-modification of cellulose nanocrystals: a green alternative towards mechanical reinforcement of ABS. *RSC Adv.* **2019**, *9*, 17417−17424.

(36) Frone, A. N.; Panaitescu, D. M.; Nicolae, C. A.; Gabor, A. R.; Trusca, R.; Casarica, A.; Stanescu, P. O.; Baciu, D. D.; Salageanu, A. Bacterial cellulose sponges obtained with green cross-linkers for tissue engineering. *Mater. Sci. Eng. C* **2020**, *110*, No. 110740.

(37) Yue, L.; Maiorana, A.; Khelifa, F.; Patel, A.; Raquez, J.-M.; Bonnaud, L.; Gross, R.; Dubois, P.; Manas-Zloczower, I. Surface-modified cellulose nanocrystals for biobased epoxy nanocomposites. *Polymer* **2018**, *134*, 155−162.

(38) Wang, L.; Hui, L.; Su, W. Superhydrophobic modification of nanocellulose based on an octadecylamine/dopamine system. *Carbohydr. Polym.* **2022**, *275*, No. 118710.

(39) Khili, F.; Borges, J. P.; Almeida, P. L.; Boukherroub, R.; Dakhlaoui, A. Extraction of Cellulose Nanocrystals with Structure I and II and Their Applications for Reduction of Graphene Oxide and Nanocomposite Elaboration. *Waste Biomass Valorization* **2019**, *10*, 1913−1927.

(40) Yadav, D.; Gohain, B. M.; Karki, S.; Ingole, P. G. A Novel Approach for the Development of Low-Cost Polymeric Thin-Film Nanocomposite Membranes for the Biomacromolecule Separation. *ACS Omega* **2022**, *7*, 47967−47985.

(41) Xie, H.; Zou, Z.; Du, H.; Zhang, X.; Wang, X.; Yang, X.; Wang, H.; Li, G.; Li, L.; Si, C. Preparation of thermally stable and surface-functionalized cellulose nanocrystals via mixed H2SO4/Oxalic acid hydrolysis. *Carbohydr. Polym.* **2019**, *223*, No. 115116.

(42) Sahoo, S. K.; Khandelwal, V.; Manik, G. Development of completely bio-based epoxy networks derived from epoxidized linseed and castor oil cured with citric acid. *Polym. Adv. Technol.* **2018**, *29*, 2080−2090.

(43) Tran, T.-N.; Di Mauro, C.; Malburet, S.; Graillot, A.; Mija, A. Dual Cross-linking of Epoxidized Linseed Oil with Combined Aliphatic/Aromatic Diacids Containing Dynamic S−S Bonds Generating Recyclable Thermosets. *ACS Appl. Bio Mater.* **2020**, *3*, 7550−7561.

(44) Díez-Pascual, A. M.; Díez-Vicente, A. L. Development of linseed oil−TiO2 green nanocomposites as antimicrobial coatings. *J. Mater. Chem. B* **2015**, *3*, 4458−4471.

(45) Li, Q.; Ni, L.; Wang, J.; Quan, H.; Zhou, Y. Establishing an ultrasound-assisted activated peroxide system for efficient and sustainable scouring-bleaching of cotton/spandex fabric. *Ultrason. Sonochem.* **2020**, *68*, No. 105220.

(46) Naffakh, M.; Díez-Pascual, A. M.; Marco, C.; Gómez, M. A.; Jiménez, I. Novel Melt-Processable Poly(ether ether ketone)(PEEK)/Inorganic Fullerene-like WS2 Nanoparticles for Critical Applications. *J. Phys. Chem. B* **2010**, *114*, 11444−11453.

(47) Díez-Pascual, A. M.; Díez-Vicente, A. L. Poly(3-hydroxybutyrate)/ZnO Bionanocomposites with Improved Mechanical, Barrier and Antibacterial Properties. *Int. J. Mol. Sci.* **2014**, *15*, 10950−10973.

(48) Song, L.; Wang, Z.; Lamm, M. E.; Yuan, L.; Tang, C. Supramolecular Polymer Nanocomposites Derived from Plant Oils and Cellulose Nanocrystals. *Macromolecules* **2017**, *50*, 7475−7483.

(49) Dhakal, H. N.; Zhang, Z. Y.; Guthrie, R.; Macmullen, J.; Bennett, N. Development of flax/carbon fibre hybrid composites for enhanced properties. *Carbohydr. Polym.* **2013**, *96*, 1−8.

(50) Saba, N.; Safwan, A.; Sanyang, M. L.; Mohammad, F.; Pervaiz, M.; Jawaid, M.; Alothman, O. Y.; Sain, M. Thermal and dynamic mechanical properties of cellulose nanofibers reinforced epoxy composites. *Int. J. Biol. Macromol.* **2017**, *102*, 822−828.

(51) Nikfar, N.; Zare, Y.; Rhee, K. Y. Dependence of mechanical performances of polymer/carbon nanotubes nanocomposites on percolation threshold. *Phys. B* **2018**, *533*, 69−75.

(52) Karki, S.; Gohain, M. B.; Yadav, D.; Ingole, P. G. Nanocomposite and bio-nanocomposite polymeric materials/membranes development in energy and medical sector: A review. *Int. J. Biol. Macromol.* **2021**, *193*, 2121−2139.

(53) Srikanth, C.; Madhu, G. M.; Kashyap, S. J. Enhanced structural, thermal, mechanical and electrical properties of nano ZTA/epoxy composites. *AIMS Mater. Sci.* **2022**, *9*, 214−235.